

Oxygen and Sodium Abundances in M13 (NGC 6205) Giants: Linking Globular Cluster Formation Scenarios, Deep Mixing, and Post–RGB Evolution

Christian I. Johnson^{1,3,4} and Catherine A. Pilachowski²

ABSTRACT

We present O, Na, and Fe abundances, as well as radial velocities, for 113 red giant branch (RGB) and asymptotic giant branch (AGB) stars in the globular cluster M13. The abundances and velocities are based on spectra obtained with the WIYN–Hydra spectrograph, and the observations range in luminosity from the horizontal branch (HB) to RGB–tip. The results are examined in the context of recent globular cluster formation scenarios. We find that M13 exhibits many key characteristics that suggest its formation and chemical enrichment are well–described by current models. Some of these observations include: the central concentration of O–poor stars, the notable decrease in [O/Fe] (but small increase in [Na/Fe]) with increasing luminosity that affects primarily the “extreme” population, the small fraction of stars with halo–like composition, and the paucity of O–poor AGB stars. In agreement with recent work, we conclude that the most O–poor M13 giants are likely He–enriched and that most (all?) O–poor RGB stars evolve to become extreme HB and AGB–manqué stars. In contrast, the “primordial” and “intermediate” population stars appear to experience standard HB and AGB evolution.

Subject headings: stars: abundances, globular clusters: general, globular clusters: individual (M13, NGC 6205). Galaxy: halo, stars: Population II

¹Department of Physics and Astronomy, UCLA, 430 Portola Plaza, Box 951547, Los Angeles, CA 90095-1547, USA; cijohnson@astro.ucla.edu

²Department of Astronomy, Indiana University, Swain West 319, 727 East Third Street, Bloomington, IN 47405-7105, USA; catyp@astro.indiana.edu

³Visiting Astronomer, Kitt Peak National Observatory, National Optical Astronomy Observatories, which is operated by the Association of Universities for Research in Astronomy, Inc. (AURA) under cooperative agreement with the National Science Foundation. The WIYN Observatory is a joint facility of the University of Wisconsin–Madison, Indiana University, Yale University, and the National Optical Astronomy Observatory.

⁴National Science Foundation Astronomy and Astrophysics Postdoctoral Fellow

1. INTRODUCTION

For many years globular clusters (GCs) were viewed as prototypical simple stellar populations containing stars of a single age and chemical composition. However, a detailed examination of GC chemistry revealed large star-to-star abundance variations of the light elements carbon through aluminum (e.g., see reviews by Kraft 1994; Gratton et al. 2004; 2012). While the anticorrelated behavior of carbon and nitrogen with increasing luminosity along the red giant branch (RGB), attributed to first dredge-up (e.g., Iben 1965) and “canonical extra mixing” (e.g., Denissenkov & Vandenberg 2003), was observed in both cluster and field stars, a peculiar pattern of enhanced N, Na, and Al abundances coupled with depleted O and Mg seemed to be only found in some cluster stars. The simultaneous anticorrelation of O and Mg with Na and Al pointed to high temperature proton-capture burning as the likely source. Unfortunately, it was not immediately clear if the processed material found in the photospheres of GC RGB stars was due to *in situ* mixing or pollution from a previous generation of more massive stars.

The comprehensive GC abundance survey by Carretta et al. (2009a,b) verified that these light element “anomalies”, in particular the O–Na anticorrelation, are likely present in *all* Galactic GCs. Additionally, several authors have now shown that the large star-to-star light element abundance variations found on the RGB are also present along the lower RGB, subgiant branch (SGB), and main-sequence turn off (e.g., Gratton et al. 2001; Cohen & Meléndez 2005; Bragaglia et al. 2010). This observation indicates that the unique abundance patterns of GCs are the result of the cluster formation and subsequent evolution rather than *in situ* processing. Recent photometric observations have discovered that many (all?) GCs exhibit multiple evolutionary sequences in their color–magnitude diagrams (e.g., see reviews by Piotto 2009; Gratton et al. 2012). Since most clusters exhibit a <0.1 dex spread in $[\text{Fe}/\text{H}]^1$ (e.g., Carretta et al. 2009c), except for a few notable cases with significant $[\text{Fe}/\text{H}]$ dispersion, the multiple photometric sequences are believed to be driven by He abundance differences. While the source of He, and subsequently the light element variations, is not known, plausible candidates include: $\sim 5\text{--}9 M_{\odot}$ asymptotic giant branch (AGB) stars (e.g., Ventura & D’Antona 2009; 2011), rapidly rotating massive main-sequence stars (e.g., Decressin et al. 2010), and massive binary stars (e.g., de Mink et al. 2009).

Although recent GC formation models incorporating winds from intermediate mass and massive stars mixed with pristine gas are able to reproduce many of the light element abundance trends unique to the cluster environment (e.g., Decressin et al. 2010; Valcarce & Catelan 2011; D’Ercole et al. 2012), the very low oxygen abundances ($[\text{O}/\text{Fe}] < -0.4$) found

¹ $[\text{A}/\text{B}] \equiv \log(N_{\text{A}}/N_{\text{B}})_{\text{star}} - \log(N_{\text{A}}/N_{\text{B}})_{\odot}$ for elements A and B.

in some GC RGB stars seems to require additional processing. While the old paradigm that the O–Na anticorrelation is entirely driven by *in situ* deep mixing in cluster RGB stars is clearly incorrect, the discovery that many GC stars are also He–rich has an important consequence for resurrecting a modified deep mixing scenario. D’Antona & Ventura (2007) showed that it is possible for a metal–poor star that is both He–rich *and* initially moderately O–poor ($[\text{O}/\text{Fe}] \sim -0.2$) and Na–rich to further deplete oxygen down to $[\text{O}/\text{Fe}] \sim -1$, without a significant change in the $[\text{Na}/\text{Fe}]$ ratio.

In light of this, M13 is a particularly illuminating case. It has long been known that M13 hosts some of the most O–poor and Na/Al–rich RGB stars of any cluster, and that these stars appear to be found preferentially near the RGB–tip (e.g., Kraft et al. 1992; Pilachowski et al. 1996; Kraft et al. 1997; Cavallo & Nagar 2000; Sneden et al. 2004; Cohen & Meléndez 2005; Johnson et al. 2005). However, the sample size of stars for which $[\text{O}/\text{Fe}]$ has been determined is ~ 5 times less than that for which $[\text{Na}/\text{Fe}]$ and $[\text{Al}/\text{Fe}]$ have been measured. Since the $[\text{O}/\text{Fe}]$ ratio may be the most sensitive indicator of deep mixing (D’Antona & Ventura 2007), in this work we have measured $[\text{O}/\text{Fe}]$ (and $[\text{Na}/\text{Fe}]$) abundances for >100 RGB and AGB stars ranging in luminosity from the RGB bump to the RGB–tip. We now use this extended sample to examine how M13’s extreme O–Na anticorrelation extension fits into the modern picture of GC formation and evolution.

2. OBSERVATIONS, DATA REDUCTION, AND ANALYSIS

All observations for this project were obtained on 2011 May 19–20 using the WIYN 3.5m telescope instrumented with the Hydra multifiber positioner and bench spectrograph. A single spectrograph setup, with wavelength coverage ranging from 6050–6350 Å, was used to obtain high signal–to–noise ratio ($\text{S}/\text{N} > 100$), moderate resolution ($R \approx 18,000$) spectra of 113 RGB and AGB stars. A color–magnitude diagram illustrating the evolutionary state of the observed stars is shown in Figure 1. All coordinates, optical photometry, and membership probabilities were taken from Cudworth & Monet (1979). Infrared photometry was taken from the 2MASS database (Skrutskie et al. 2006). To ensure membership, we only observed targets with $P > 70\%$.

The data reduction and analysis closely follow the techniques outlined in Johnson et al. (2005) and Johnson & Pilachowski (2010). To briefly summarize, effective temperature (T_{eff}) and surface gravity ($\log(g)$) were set for each star using dereddened V and K_s photometry. We initially assumed $[\text{Fe}/\text{H}] = -1.50$ and a microturbulence (v_t) value of 2 km s^{-1} and interpolated within the α –enhanced, AODFNEW grid of ATLAS9 model atmospheres (Castelli et al. 1997). The final model metallicity was set as the average $[\text{Fe}/\text{H}]$ derived from

Fe I and Fe II lines, and v_t was set by removing any trend in Fe I abundance versus line strength.

Abundances for Fe I and Fe II were derived via equivalent width measurements while O and Na abundances were determined through spectrum synthesis. All abundances were calculated using the 2010 version of the LTE line analysis code MOOG (Sneden et al. 1973). The linelist was the same as that used in Johnson & Pilachowski (2010). A summary of all derived model atmosphere parameters, coordinates, abundances, and radial velocities is provided in Table 1.

3. BASIC RESULTS

Despite exhibiting large light element abundance variations, M13 has always been characterized by a single metallicity ($[\text{Fe}/\text{H}] \sim -1.5$). We find in agreement with past large sample studies (e.g., Pilachowski et al. 1996; Sneden et al. 2004; Cohen & Meléndez 2005) that M13 is moderately metal-poor and exhibits small star-to-star variation in $[\text{Fe}/\text{H}]$. In particular, we find $\langle [\text{Fe}/\text{H}] \rangle = -1.57$ ($\sigma = 0.07$), with an average agreement between $[\text{Fe}/\text{H}]$ derived by Fe I and Fe II (in the sense $[\text{FeI}/\text{H}] - [\text{FeII}/\text{H}]$) of -0.04 ($\sigma = 0.15$). The Fe I abundances are based on an average of 27 lines ($\sigma = 4$), with a typical line-to-line dispersion of 0.13 dex ($\sigma = 0.02$). In contrast, the Fe II abundances are based on 1–3 lines, with an average line-to-line dispersion of 0.11 dex ($\sigma = 0.07$). While the agreement between $[\text{FeI}/\text{H}]$ and $[\text{FeII}/\text{H}]$ is good for most stars, Table 1 shows that there is some disparity for the coolest, most luminous giants. This is likely due to a combination of mass loss, variability (if $V \lesssim 12.5$; Kopacki et al. 2003), model atmosphere deficiencies, and NLTE effects.

In agreement with past work (e.g., Pilachowski et al. 1996; Kraft et al. 1997; Cavallo & Nagar 2000; Sneden et al. 2004; Cohen & Meléndez 2005; Johnson et al. 2005), we find large star-to-star abundance variations for both $[\text{O}/\text{Fe}]$ and $[\text{Na}/\text{Fe}]$ and reproduce the well-known O–Na anticorrelation (see Figure 2). The $[\text{O}/\text{Fe}]^2$ ratio ranges from -1.05 to $+0.74$, with an average $[\text{O}/\text{Fe}] = +0.06$ ($\sigma = 0.34$). Similarly, $[\text{Na}/\text{Fe}]$ ranges from -0.66 to $+0.71$, with an average of $[\text{Na}/\text{Fe}] = +0.23$ ($\sigma = 0.24$). For Na, the average measurement error is 0.08 dex ($\sigma = 0.07$). While the O abundance is derived solely from the 6300 Å [O I] line, the typical synthesis fitting uncertainty is $\lesssim 0.1$ dex.

We did not apply any NLTE corrections to the $[\text{Na}/\text{Fe}]$ abundances. Although departures from LTE are expected for cool, metal-poor giants, the magnitude of the corrections

²Note that we measured $[\text{O}/\text{Fe}]$ relative to $[\text{Fe}/\text{H}]_{\text{avg}}$, rather than $[\text{FeII}/\text{H}]$.

likely do not exceed ~ 0.1 dex for the 6154/6160 Å Na I lines (e.g., Lind et al. 2011). The results presented here indicate a correlation between luminosity and the O–Na anticorrelation, and it is important to ensure this result is not purely a consequence of NLTE effects or model atmosphere deficiencies. While it is difficult to completely rule out these effects, we note that: (1) abundance analyses of evolved RGB stars in the similar metallicity GC M3 do *not* find a correlation between O/Na abundance and luminosity (e.g., Sneden et al. 2004; Cohen & Meléndez 2005) and (2) as can be seen in Figure 3 there is a clear variation in O/Na line strength among stars of similar luminosity.

Following the typical naming scheme for GC sub-populations (e.g., Carretta et al. 2009a), in Figures 1–2 we differentiate M13 stars into the “primordial”, “intermediate”, and “extreme” populations based on their [O/Fe] and [Na/Fe] abundances.³ We find that the primordial, intermediate, and extreme populations constitute 15%, 63%, and 22% of our sample, respectively, which is typical for Galactic GCs (e.g., Carretta et al. 2009a). Interestingly, as can be seen in Figures 1–2, the extreme population seems to differentiate itself by consisting of stars predominantly near the RGB–tip, a result noted in many past studies (e.g., Kraft et al. 1997), and is the most centrally concentrated. Additionally, we note that none of the AGB stars in our sample are particularly O–poor (see also Pilachowski et al. 1996). We discuss the implications of these observations further in §4.

In addition to determining abundance ratios, we also measured radial velocities for all stars using the IRAF *fxcor* routine. We find an average heliocentric radial velocity (RV) of -244.7 km s⁻¹ ($\sigma=6.1$), which is in good agreement with past studies (e.g., Lupton et al. 1987). The average measurement error is ~ 0.2 km s⁻¹. The small star–to–star velocity dispersion indicates that all of our observed targets are likely cluster members. Interestingly, the extreme population exhibits an average RV that is ~ 2 km s⁻¹ larger than the primordial and intermediate stars, which have identical average RVs. However, this may be due to the fact that most extreme population stars are near the RGB–tip and therefore likely to be variables (e.g., Kopacki et al. 2003).

4. DISCUSSION AND CONCLUSIONS

As mentioned in §1, recent models predict that GCs likely form in (at least) two distinct episodes. In this scenario, the first star formation event produces stars with halo–like composition (the primordial population), and then the $\gtrsim 5 M_{\odot}$ progeny of the first genera-

³Note that our definitions are slightly different than those used in previous studies. Here we designate extreme stars by [O/Fe] < -0.15, primordial stars by [Na/Fe] < +0.00, and the remainder as intermediate stars.

tion pollute the cluster with material heavily processed by high temperature proton–capture burning, including newly synthesized He. This new material may be funneled to the cluster core (e.g., D’Ercole et al. 2008) where the second generation stars (intermediate and extreme populations) form; however, it appears that some dilution with pristine gas is required to reproduce the observed light element abundance trends (e.g., Prantzos et al. 2007; D’Ercole et al. 2011). Some implications of this scenario are that: (1) the primordial population is preferentially stripped relative to the second generation stars, (2) the second generation stars may be significantly He–enhanced and more centrally concentrated, and (3) the extra He, in addition to producing multiple evolutionary sequences in cluster color–magnitude diagrams, may cause some stars to experience *in situ* deep mixing above the RGB bump and/or cause the most He–rich stars to become RGB–manqué, AGB–manqué, or extreme blue horizontal branch (HB) stars. As we discuss below, M13 appears to exhibit many of these characteristics.⁴

4.1. Supporting Observations of Globular Cluster Formation Models

We noted in §3 that the primordial population constitutes a considerably smaller fraction of stars in M13 (15%) than the intermediate and extreme populations. This is consistent with the cluster formation scenario mentioned above where a significant percentage (up to $\sim 90\%$) of first generation but not second generation stars are lost early in the formation process. Although our estimate is somewhat lower than the 34% primordial fraction determined by Carretta et al. (2009a; their Table 5), we note that there is typically no clear separation between the primordial and intermediate populations. However, the dominance of the intermediate population in M13 strongly suggests that its formation and chemical enrichment followed the same path as other halo GCs.

Similarly, we show in Figure 2 that the extreme population appears to be marginally more centrally concentrated than the primordial and intermediate stars. This is supported by the results of two–sided KS tests, which indicate that the primordial and intermediate populations trace the same radial distribution (KS–prob=0.9018) but the extreme population is different than both (KS–prob_{P,E}=0.1603; KS–prob_{I,E}=0.0935). Although the statistical significance is marginal, we note that similar results have been found in a few other clusters where the central concentration of extreme stars is supported by independent observations of radial changes in the color–magnitude diagram (e.g., Carretta et al. 2010; Lardo et al.

⁴Interestingly, multiple sequences in M13 color–magnitude diagrams have yet to be found (see Sandquist et al. 2010 for a recent update.)

2011). While the dynamical evolution of a GC is expected to smear out the radial profile and uniformly mix the various populations after a Hubble time (e.g., Decressin et al. 2010; but see also Bekki 2010), the fact that M13 and other clusters still show a semblance of the extreme stars being centrally concentrated is evidence in support of current cluster formation models. In this light, ω Cen is a particularly illustrative example. Since the core relaxation time is similar to the cluster age, ω Cen likely preserves early formation history clues. In fact, Johnson & Pilachowski (2010) and Gratton et al. (2011) find a clear composition dependence on radial location, with the extreme stars being the most centrally concentrated and the primordial stars the least.

4.2. Connecting to the New Deep Mixing Model

Although we now know that the historical argument relating *in situ* deep mixing and the O–Na anticorrelation is incorrect, a modified version has recently been resurrected to explain cluster RGB stars with $[O/Fe] \lesssim -0.4$ (e.g., D’Antona & Ventura 2007). As mentioned in §1, predicted yields from both $>5 M_{\odot}$ AGB and massive main–sequence stars generally fail to produce second generation stars with $[O/Fe] \lesssim -0.4$ and thus a secondary process is required.

Interestingly, our M13 observations (and those of past authors) appear to verify the predictions of the D’Antona & Ventura (2007) model (see also Figure 1): (1) all of the known stars with $[O/Fe] \lesssim -0.4$ are located well above the RGB bump, (2) in general there is a monotonic decrease in $[O/Fe]$ with increasing luminosity for the extreme population, and (3) at the highest luminosity there is a large difference in $\langle [O/Fe] \rangle$ between the extreme and intermediate populations but only ~ 0.1 dex increase in $\langle [Na/Fe] \rangle$ for the extreme stars. We believe the requirements to induce deep mixing (enhanced He and initially low $[O/Fe]$) are also met for the extreme M13 giants.

Figure 1 shows that (with one exception) the lowest $[O/Fe]$ ratio found at $\log(L/L_{\odot}) < 2.8$ is consistently at $[O/Fe] \sim -0.3$. Note that this is consistent with the Cohen & Meléndez (2005) observations that do not find stars below the RGB bump with $[O/Fe] < -0.2$. This supports the idea that the low $[O/Fe]$ values found only in the brightest M13 RGB stars is an evolutionary effect and that significant O–depletion does not occur at low RGB luminosities. With regard to He–enhancement, we do not have direct He measurements for these stars but note that the most Na/Al–rich (and thus O–poor) stars in ω Cen (Dupree et al. 2011) and NGC 2808 (Pasquini et al. 2012) have enhanced He. We also find ancillary evidence, similar to that found by Carretta et al. (2006) in NGC 2808, in support of He–enrichment from the increase in $[Fe/H]$ from -1.58 in the intermediate population to -1.54 in the extreme

population.⁵ However, we note that Sandquist et al. (2010) does not find significant evidence for He–enrichment in M13. On the other hand, if the O–poor stars are He–rich then the fact that deep mixing appears to be activated at a single luminosity ($\log(L/L_{\odot})\sim 2.8$) may be evidence in support of the extreme stars having a small He spread. This is qualitatively in agreement with photometric studies that often find discrete populations in cluster color–magnitude diagrams rather than a spread (e.g., Piotto 2009).

4.3. Composition and Post–RGB Evolution

In the scenario described above, the most He–rich stars likely undergo deep mixing that has the observational effect of decreasing $[O/Fe]$; however, it also increases the envelope He abundance to as much as $Y=0.5$ (e.g., D’Antona & Ventura 2007). Since He–enhancement may be strongly manifest in HB and AGB evolution, we can look to these stars for clues regarding He–enhancement and RGB evolution. One of the most notable features of Figure 1, which has been shown previously with Na abundances (e.g., Pilachowski et al. 1996), is the lack of extreme stars on the AGB.⁶ Since we find the extreme stars to constitute $\sim 20\%$ of M13’s total population, we should expect to find ~ 2 – 3 super O–poor AGB stars in our sample. Interestingly, we find that only the primordial and intermediate AGB stars are present in about the same proportion as on the RGB. Following similar results in other GCs (e.g., Norris et al. 1981; Campbell et al. 2010; Gratton et al. 2010), we conclude that in M13 only the primordial and intermediate populations undergo standard HB and AGB evolution.

What about the fate of the extreme population? M13 is known to contain a bimodal and extreme blue HB (e.g., see Sandquist et al. 2010 and references therein). Circumstantial evidence supports the idea that the “faint peak” population of HB stars, which have very high T_{eff} , were also once the most O–poor giants on the RGB. In particular, the fraction of faint peak relative to total HB stars is about equal to the fraction of extreme to total RGB stars. The faint peak stars were also found by Sandquist et al. (2010) to be more centrally concentrated than the “intermediate” and “bright peak” populations. Furthermore, the Sandquist et al. (2010) data indicate that: (1) the fraction of AGB–manqué to total AGB

⁵We caution the reader on this point because the $[Fe/H]$ difference is small and several of the extreme population stars are known to be variable.

⁶With the present data we are unable to differentiate AGB and RGB stars near the RGB–tip. However, we expect most, if not all, of the stars near the RGB–tip to be first ascent giants because of the short evolutionary timescale of AGB stars.

stars is $\sim 23\%$ and (2) the origin of the AGB–manqué stars is likely the bluest part of the HB. Additionally, Peterson et al. (1995) provide $[\text{O}/\text{Fe}]$ abundances for cool HB stars in M13 and do not find any with $[\text{O}/\text{Fe}] < 0$. All of these observations suggest that the extreme RGB stars evolve from the RGB to the bluest end of the HB and then become AGB–manqué stars.

4.4. Final Thoughts

The results presented here have allowed us to re–examine M13 in light of recent advances in our understanding of GC formation. M13 may be well explained by the new “standard” picture in which first generation stars with halo–like composition are preferentially lost early in the cluster evolution, and a second, more enriched population forms in the cluster center from gas processed and ejected by $>5 M_{\odot}$ first generation stars. For M13, this has the effect of instigating *in situ* deep mixing in the most He–rich giants and perhaps causing them to terminate their evolution before ascending the AGB. In fact, proper modeling of the warmest HB stars in clusters like M13 may require considering composition changes to the RGB envelope due to *in situ* mixing. However, two outstanding issues remain: (1) will precise photometry in the inner part of the cluster finally reveal multiple populations and (2) are some M13 stars actually He–rich?

This material is based upon work supported by the National Science Foundation under award No. AST–1003201 to CIJ. CAP gratefully acknowledges support from the Daniel Kirkwood Research Fund at Indiana University.

REFERENCES

- Bekki, K. 2010, ApJ, 724, L99
- Bragaglia, A., Carretta, E., Gratton, R. G., et al. 2010, ApJ, 720, L41
- Campbell, S. W., Yong, D., Wylie-de Boer, E. C., et al. 2010, Mem. Soc. Astron. Italiana, 81, 1004
- Carretta, E., Bragaglia, A., Gratton, R. G., et al. 2006, A&A, 450, 523
- Carretta, E., Bragaglia, A., Gratton, R. G., et al. 2009a, A&A, 505, 117
- Carretta, E., Bragaglia, A., Gratton, R., & Lucatello, S. 2009b, A&A, 505, 139

- Carretta, E., Bragaglia, A., Gratton, R., D’Orazi, V., & Lucatello, S. 2009c, *A&A*, 508, 695
- Carretta, E., Bragaglia, A., D’Orazi, V., Lucatello, S., & Gratton, R. G. 2010, *A&A*, 519, A71
- Castelli, F., Gratton, R. G., & Kurucz, R. L. 1997, *A&A*, 318, 841
- Cavallo, R. M., & Nagar, N. M. 2000, *AJ*, 120, 1364
- Cohen, J. G., & Meléndez, J. 2005, *AJ*, 129, 303
- Cudworth, K. M., & Monet, D. G. 1979, *AJ*, 84, 774
- D’Antona, F., & Ventura, P. 2007, *MNRAS*, 379, 1431
- D’Ercole, A., Vesperini, E., D’Antona, F., McMillan, S. L. W., & Recchi, S. 2008, *MNRAS*, 391, 825
- D’Ercole, A., D’Antona, F., & Vesperini, E. 2011, *MNRAS*, 415, 1304
- D’Ercole, A., D’Antona, F., Carini, R., Vesperini, E., & Ventura, P. 2012, *MNRAS*, 2921
- de Mink, S. E., Pols, O. R., Langer, N., & Izzard, R. G. 2009, *A&A*, 507, L1
- Decressin, T., Baumgardt, H., Charbonnel, C., & Kroupa, P. 2010, *A&A*, 516, A73
- Denissenkov, P. A., & Vandenberg, D. A. 2003, *ApJ*, 593, 509
- Dupree, A. K., Strader, J., & Smith, G. H. 2011, *ApJ*, 728, 155
- Gratton, R. G., Bonifacio, P., Bragaglia, A., et al. 2001, *A&A*, 369, 87
- Gratton, R., Sneden, C., & Carretta, E. 2004, *ARA&A*, 42, 385
- Gratton, R. G., D’Orazi, V., Bragaglia, A., Carretta, E., & Lucatello, S. 2010, *A&A*, 522, A77
- Gratton, R. G., Johnson, C. I., Lucatello, S., D’Orazi, D’Orazi, V., & Pilachowski, C. 2011, *A&A*, 534, A72
- Gratton, R. G., Carretta, E., & Bragaglia, A. 2012, *A&A Rev.*, 20, 50
- Iben, I., Jr. 1965, *ApJ*, 142, 1447
- Johnson, C. I., Kraft, R. P., Pilachowski, C. A., et al. 2005, *PASP*, 117, 1308

- Johnson, C. I., & Pilachowski, C. A. 2010, *ApJ*, 722, 1373
- Kadla, Z. I. 1966, *Comm. Pulkova Obs.*, 24, No. 181, 93
- Kopacki, G., Kołaczkowski, Z., & Pigulski, A. 2003, *A&A*, 398, 541
- Kraft, R. P., Sneden, C., Langer, G. E., & Prosser, C. F. 1992, *AJ*, 104, 645
- Kraft, R. P. 1994, *PASP*, 106, 553
- Kraft, R. P., Sneden, C., Smith, G. H., et al. 1997, *AJ*, 113, 279
- Lardo, C., Bellazzini, M., Pancino, E., et al. 2011, *A&A*, 525, A114
- Lind, K., Asplund, M., Barklem, P. S., & Belyaev, A. K. 2011, *A&A*, 528, A103
- Ludendorf, H. 1905, *Publ. Astrophys. Obs. Potsdam*, 15, No. 50
- Lupton, R. H., Gunn, J. E., & Griffin, R. F. 1987, *AJ*, 93, 1114
- Norris, J., Cottrell, P. L., Freeman, K. C., & Da Costa, G. S. 1981, *ApJ*, 244, 205
- Pasquini, L., Mauas, P., Käuffl, H. U., & Cacciari, C. 2011, *A&A*, 531, A35
- Peterson, R. C., Rood, R. T., & Crocker, D. A. 1995, *ApJ*, 453, 214
- Pilachowski, C. A., Sneden, C., Kraft, R. P., & Langer, G. E. 1996, *AJ*, 112, 545
- Piotto, G. 2009, *IAU Symposium*, 258, 233
- Prantzos, N., Charbonnel, C., & Iliadis, C. 2007, *A&A*, 470, 179
- Sandquist, E. L., Gordon, M., Levine, D., & Bolte, M. 2010, *AJ*, 139, 2374
- Skrutskie, M. F., Cutri, R. M., Stiening, R., et al. 2006, *AJ*, 131, 1163
- Sneden, C. 1973, *ApJ*, 184, 839
- Sneden, C., Kraft, R. P., Guhathakurta, P., Peterson, R. C., & Fulbright, J. P. 2004, *AJ*, 127, 2162
- Valcarce, A. A. R., & Catelan, M. 2011, *A&A*, 533, A120
- Ventura, P., & D’Antona, F. 2009, *A&A*, 499, 835
- Ventura, P., & D’Antona, F. 2011, *MNRAS*, 410, 2760

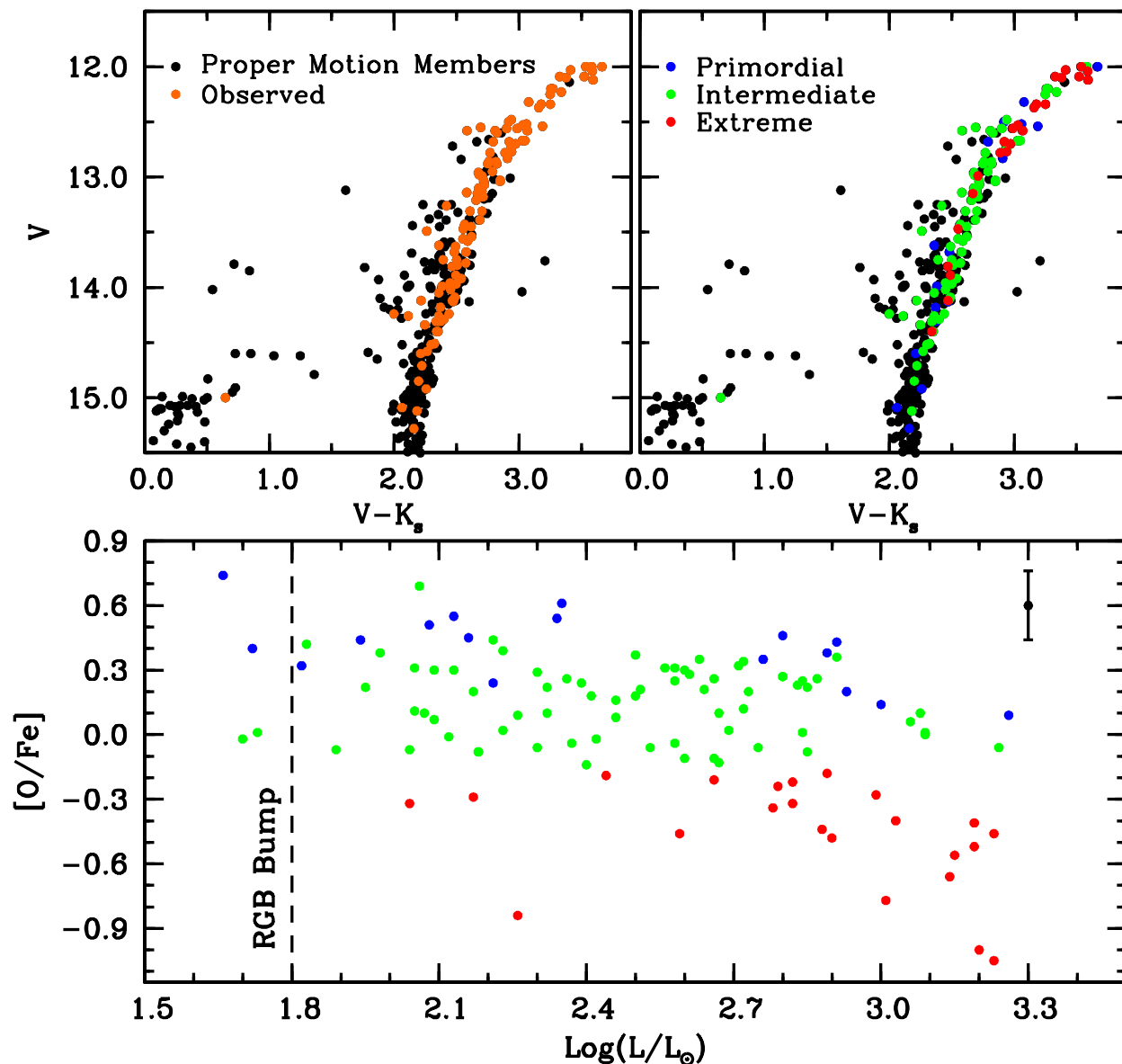


Fig. 1.— The top left panel shows a V versus $V-K_s$ color-magnitude diagram indicating the stars observed for this program. The top right panel shows the same stars differentiated by chemical composition (see also §3). The bottom panel plots $[O/Fe]$ versus $\log(L/L_\odot)$. The different color symbols have the same meaning as in the top right panel.

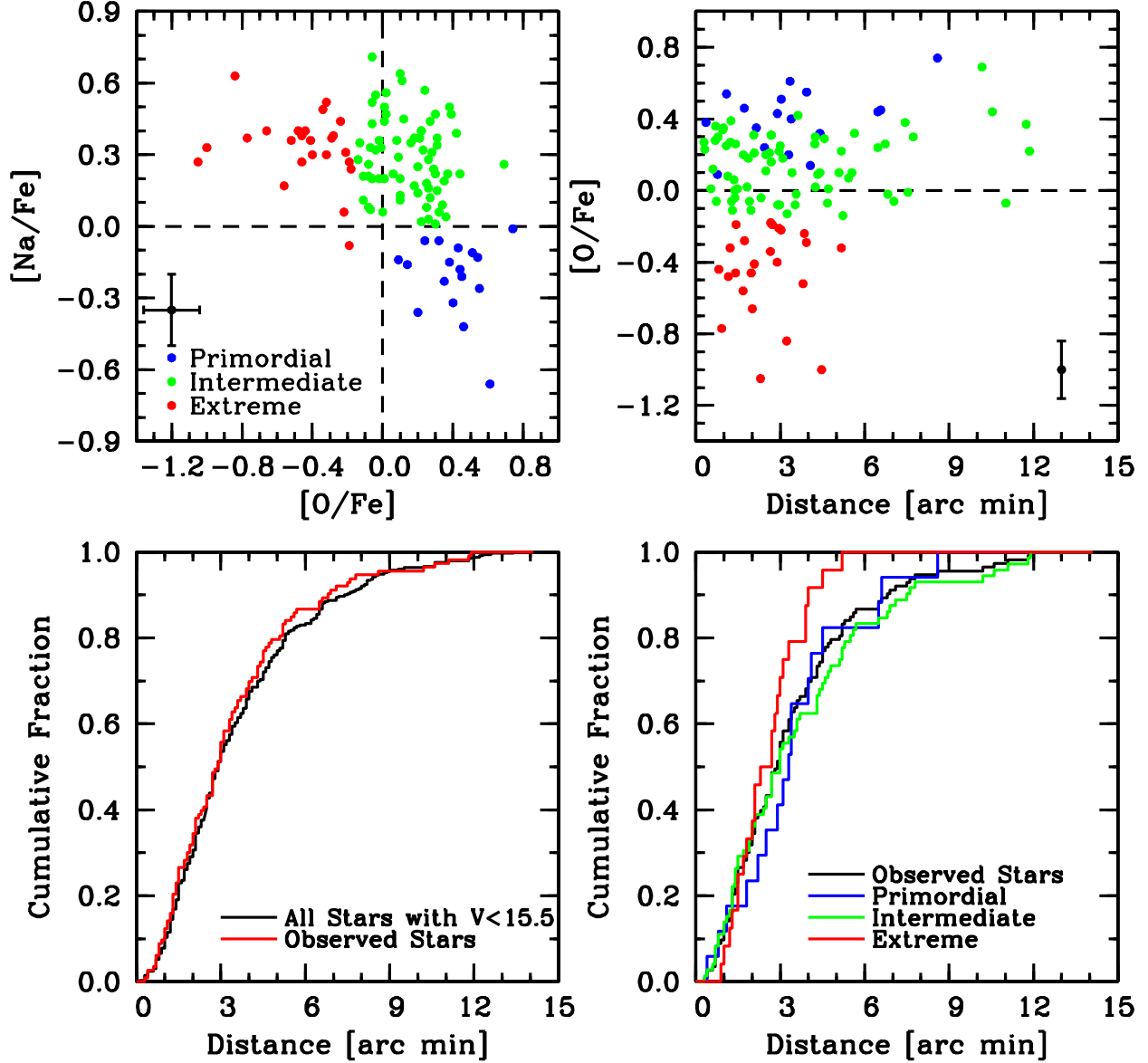


Fig. 2.— The top left panel plots $[\text{Na}/\text{Fe}]$ versus $[\text{O}/\text{Fe}]$, and the top right panel shows $[\text{O}/\text{Fe}]$ versus distance from the cluster center. The bottom left panel illustrates the cumulative fraction as a function of radial distance for all proper motion members (solid black line) and our observed distribution (solid red line). The bottom right panel compares the cumulative distribution of our observations based on composition.

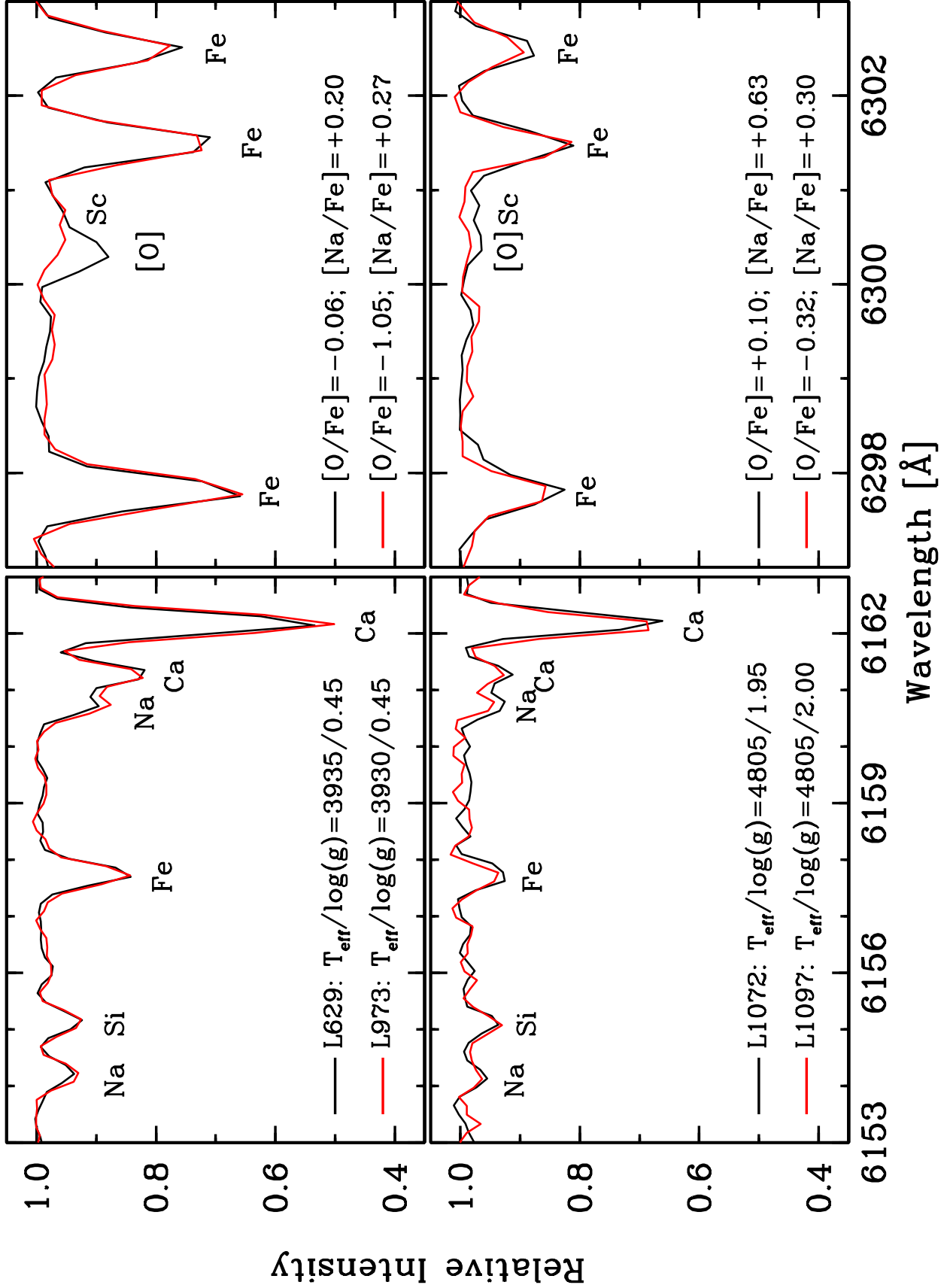


Fig. 3.— Sample spectra for two sets of stars with similar $T_{\text{eff}}/\log(g)$ but different $[\text{O}/\text{Fe}]$ and $[\text{Na}/\text{Fe}]$ abundances.

Table 1. Basic Data and Results

Star Name ^a	Alt. Name	RA J2000	DEC J2000	V	K _S	log(L/L _⊙)	T _{eff} (K)	log(g) (cgs)	[Fe/H] avg.	vt km s ⁻¹	[FeI/H]	[FeII/H]	[O/Fe]	[Na/Fe]	RV km s ⁻¹
L 324	V11	250.402711	36.443214	12.00	8.465	3.23	3955	0.45	-1.50	2.50	-1.67	-1.32	-0.46	+0.27	-242.7
L 598	...	250.424834	36.447735	12.00	8.335	3.26	3895	0.40	-1.44	2.20	-1.57	-1.31	+0.09	-0.14	-257.6
L 629	...	250.427326	36.448975	12.00	8.418	3.24	3935	0.45	-1.57	2.15	-1.71	-1.42	-0.06	+0.20	-232.4
L 194	II-90	250.383343	36.474979	12.03	8.616	3.19	4015	0.50	-1.49	2.30	-1.53	-1.45	-0.41	+0.36	-239.3
L 973	I-48	250.462198	36.481819	12.04	8.452	3.23	3930	0.45	-1.50	2.35	-1.68	-1.32	-1.05	+0.27	-249.5
L 835	V15	250.445965	36.432686	12.09	8.763	3.14	4060	0.60	-1.50	2.15	-1.56	-1.43	-0.66	+0.40	-258.3
L 954	IV-25	250.459624	36.404362	12.09	8.568	3.19	3960	0.50	-1.48	2.30	-1.62	-1.34	-0.52	+0.36	-251.9
L 940	...	250.457090	36.463585	12.10	8.722	3.15	4030	0.55	-1.53	2.00	-1.62	-1.44	-0.56	+0.17	-246.5
L 70	II-67	250.348070	36.504818	12.12	8.527	3.20	3925	0.50	-1.45	2.35	-1.66	-1.24	-1.00	+0.33	-241.8
L 199	III-63	250.385576	36.411789	12.20	8.944	3.08	4095	0.65	-1.61	2.00	-1.66	-1.56	+0.10	+0.20	-247.7
L 853	...	250.447669	36.474579	12.20	8.927	3.09	4090	0.65	-1.51	2.00	-1.59	-1.43	+0.01	+0.20	-246.5
L 261	...	250.394873	36.466564	12.23	8.891	3.09	4050	0.65	-1.59	2.00	-1.66	-1.52	+0.00	+0.06	-233.9
L 262	...	250.395118	36.455494	12.25	9.000	3.06	4100	0.70	-1.58	2.00	-1.68	-1.48	+0.06	+0.22	-239.7
L 72	III-73	250.350357	36.425182	12.32	9.242	3.00	4000	0.65	-1.59	2.30	-1.79	-1.38	+0.14	-0.16	+243.0
L 240	II-34	250.391365	36.501595	12.34	9.088	3.03	4100	0.70	-1.42	2.00	-1.54	-1.30	-0.40	+0.30	+236.6
L 481	...	250.415993	36.474773	12.34	9.163	3.01	4145	0.75	-1.49	1.90	-1.56	-1.41	-0.77	+0.37	+238.1
L 250	...	250.393700	36.443489	12.37	9.211	2.99	4155	0.80	-1.58	1.95	-1.66	-1.49	-0.28	+0.38	-247.7
L 384	...	250.408606	36.463726	12.48	9.541	2.91	4295	0.90	-1.61	1.75	-1.53	-1.68	+0.36	+0.04	-243.1
L 465	...	250.415078	36.460598	12.50	9.583	2.89	4310	0.95	-1.64	1.90	-1.56	-1.71	+0.38	-0.15	-250.1
L 96	II-76	250.362885	36.466747	12.52	9.460	2.91	4215	0.90	-1.63	2.00	-1.76	-1.49	+0.43	-0.09	-236.3
L 845	...	250.446598	36.462189	12.53	9.499	2.90	4235	0.90	-1.57	1.85	-1.58	-1.56	-0.48	+0.40	-257.4
L 745	I-13	250.436927	36.514297	12.54	9.351	2.93	4135	0.85	-1.55	2.00	-1.66	-1.43	+0.20	-0.36	-242.7
L 584	...	250.423848	36.455242	12.55	9.857	2.83	4480	1.05	-1.63	1.85	-1.49	-1.77	+0.23	+0.32	-251.7
L 296	...	250.398768	36.446945	12.56	9.659	2.87	4320	0.95	-1.71	2.30	-1.78	-1.63	+0.26	+0.28	-246.6
L 367	...	250.406780	36.465542	12.56	9.575	2.88	4260	0.95	-1.57	1.85	-1.60	-1.53	-0.44	+0.40	-244.2
L 316	III-59	250.401230	36.419556	12.58	9.513	2.89	4210	0.90	-1.62	2.00	-1.65	-1.59	-0.18	+0.24	-238.7
L 549	...	250.421200	36.465279	12.58	9.996	2.80	4570	1.15	-1.62	1.75	-1.46	-1.78	+0.27	+0.44	-253.6
L 674	...	250.430845	36.454346	12.58	9.771	2.84	4390	1.05	-1.62	1.85	-1.58	-1.66	+0.01	+0.44	-244.2
L 398	...	250.409644	36.475033	12.60	9.775	2.84	4375	1.05	-1.55	1.85	-1.51	-1.59	+0.25	+0.08	-235.7
L 244	III-52	250.393224	36.418015	12.67	9.622	2.85	4220	0.95	-1.62	1.90	-1.66	-1.58	-0.08	+0.26	-245.8
L 252	II-33	250.393145	36.503727	12.67	9.643	2.85	4235	0.95	-1.60	1.90	-1.65	-1.55	+0.22	+0.02	-238.0
L 830	...	250.445026	36.451096	12.68	9.758	2.82	4305	1.00	-1.59	1.90	-1.59	-1.58	-0.32	+0.52	-247.6
L 938	IV-53	250.456950	36.452896	12.68	9.887	2.80	4400	1.10	-1.63	1.95	-1.58	-1.68	+0.46	-0.42	-239.7
L 158	II-57	250.377230	36.495411	12.70	9.727	2.82	4270	1.00	-1.58	1.90	-1.65	-1.51	-0.22	+0.06	-246.2

Table 1—Continued

Star Name ^a	Alt. Name	RA J2000	DEC J2000	V	K _S	log(L/L _☉)	T _{eff} (K)	log(g) (cgs)	[Fe/H] avg.	vt km s ⁻¹	[FeI/H]	[FeII/H]	[O/Fe]	[Na/Fe]	RV km s ⁻¹
L 666	...	250.430458	36.440987	12.73	9.794	2.80	4295	1.00	-1.57	1.75	-1.54	-1.60	+0.27	+0.12	-251.7
L 77	III-18	250.352673	36.429165	12.77	9.830	2.79	4295	1.05	-1.62	1.95	-1.63	-1.60	-0.24	+0.44	-233.8
L 169	III-37	250.379465	36.432983	12.78	9.891	2.78	4330	1.05	-1.52	1.80	-1.55	-1.48	-0.34	+0.49	-246.7
L 825	...	250.444365	36.472321	12.78	10.011	2.75	4420	1.15	-1.55	1.80	-1.54	-1.55	-0.06	+0.43	-241.8
L 353	II-40	250.405233	36.493576	12.83	9.923	2.76	4315	1.10	-1.58	2.00	-1.67	-1.49	+0.35	-0.23	-237.2
L 594	...	250.424539	36.470486	12.86	10.099	2.72	4425	1.15	-1.57	1.80	-1.53	-1.60	+0.12	+0.45	-252.3
L 777	I-24	250.439463	36.499626	12.86	10.045	2.73	4385	1.15	-1.57	1.85	-1.58	-1.55	+0.20	+0.14	-244.6
L 1073	...	250.503562	36.392738	12.88	10.130	2.71	4430	1.15	-1.64	2.10	-1.72	-1.56	+0.32	+0.06	-250.9
L 754	...	250.438238	36.470348	12.88	10.058	2.72	4380	1.15	-1.60	1.80	-1.62	-1.58	+0.34	+0.09	-242.9
L 198	...	250.384773	36.459621	12.95	10.163	2.69	4405	1.20	-1.53	1.65	-1.47	-1.59	+0.02	+0.47	-247.6
L 687	IV-15	250.433291	36.376057	12.96	10.285	2.67	4490	1.25	-1.65	2.00	-1.73	-1.57	+0.10	+0.13	-251.0
L 863	I-42	250.448676	36.485596	12.98	10.299	2.66	4490	1.25	-1.59	1.80	-1.52	-1.66	-0.11	+0.11	-248.2
L 1023	IV-61	250.475473	36.435909	12.99	10.285	2.66	4470	1.25	-1.50	1.75	-1.48	-1.51	-0.21	+0.31	-244.6
L 877	I-50	250.450037	36.498093	13.03	10.313	2.64	4460	1.25	-1.66	1.90	-1.64	-1.68	+0.21	+0.37	-245.7
L 919	IV-28	250.455285	36.413113	13.03	10.181	2.67	4360	1.20	-1.62	1.95	-1.62	...	-0.13	+0.35	-255.6
K 656	...	250.561750	36.455540	13.04	10.191	2.66	4360	1.20	-1.57	1.85	-1.64	-1.49	+0.26	+0.03	-242.2
L 343	...	250.404518	36.453026	13.07	10.348	2.63	4455	1.25	-1.60	1.75	-1.56	-1.63	+0.35	+0.19	-241.8
L 592	...	250.424562	36.471794	13.10	10.423	2.61	4490	1.30	-1.68	1.85	-1.65	-1.70	+0.28	+0.31	-243.1
L 476	...	250.415991	36.448318	13.13	10.426	2.60	4470	1.30	-1.62	1.90	-1.60	-1.63	+0.30	+0.22	-230.1
L 269	...	250.395629	36.458511	13.14	10.457	2.60	4485	1.30	-1.65	1.75	-1.81	-1.48	-0.11	+0.21	-242.7
L 948	IV-35	250.458472	36.419598	13.14	10.559	2.58	4565	1.35	-1.64	1.90	-1.70	-1.58	+0.25	+0.18	-246.0
L 967	I-86	250.460928	36.471931	13.15	10.482	2.59	4500	1.35	-1.55	1.70	-1.52	-1.57	-0.46	+0.38	-256.0
L 1030	I-77	250.477617	36.456387	13.18	10.482	2.58	4475	1.30	-1.61	1.75	-1.53	-1.68	+0.31	+0.15	-255.3
L 644	...	250.428298	36.483116	13.18	10.467	2.58	4460	1.30	-1.62	1.70	-1.57	-1.66	-0.04	+0.32	-233.1
L 773	I-23	250.439378	36.503170	13.21	10.554	2.56	4510	1.35	-1.66	1.90	-1.76	-1.56	+0.31	+0.34	-236.1
L 956	...	250.459008	36.471024	13.26	10.841	2.50	4720	1.50	-1.63	1.45	-1.67	-1.59	+0.18	+0.37	-242.6
K 228	J 3	250.277032	36.470470	13.31	10.606	2.53	4470	1.35	-1.45	1.75	-1.52	-1.37	-0.06	+0.52	-249.0
L 176	II-87	250.380242	36.467278	13.31	10.702	2.51	4550	1.40	-1.61	1.75	-1.58	-1.63	+0.21	+0.37	-240.4
K 188	A1	250.179091	36.461632	13.39	10.704	2.50	4485	1.40	-1.52	1.70	-1.58	-1.46	+0.37	+0.22	-243.7
L 436	...	250.412601	36.443130	13.43	10.865	2.46	4580	1.50	-1.78	1.60	-1.76	-1.79	+0.08	+0.36	-233.0
L 114	III-7	250.368221	36.451057	13.45	10.835	2.46	4540	1.45	-1.61	1.80	-1.61	-1.60	+0.16	+0.35	-250.6
L 370	...	250.407394	36.440029	13.47	10.917	2.44	4590	1.50	-1.66	1.60	-1.69	-1.63	-0.19	+0.27	-243.9
L 1043	BAUM 13	250.480977	36.557415	13.49	11.229	2.39	4885	1.65	-1.67	1.80	-1.64	-1.70	+0.24	+0.57	-244.6
L 766	I-12	250.438708	36.518581	13.54	10.920	2.42	4540	1.50	-1.63	1.70	-1.63	-1.63	-0.02	+0.20	-247.9

Table 1—Continued

Star Name ^a	Alt. Name	RA J2000	DEC J2000	V	K _S	log(L/L _⊙)	T _{eff} (K)	log(g) (cgs)	[Fe/H] avg.	vt km s ⁻¹	[FeI/H]	[FeII/H]	[O/Fe]	[Na/Fe]	RV km s ⁻¹
L 172	III-45	250.380327	36.421734	13.56	11.008	2.41	4595	1.55	-1.58	1.60	-1.54	-1.61	+0.18	+0.17	-233.9
L 26	J38	250.320860	36.429989	13.58	10.991	2.40	4565	1.55	-1.51	1.60	-1.51	-1.50	-0.14	+0.28	-241.8
L 168	II-28	250.378456	36.503632	13.62	11.261	2.35	4780	1.65	-1.64	1.90	-1.67	-1.60	+0.61	-0.66	-245.6
L 193	II-94	250.382611	36.482044	13.63	11.139	2.37	4650	1.60	-1.56	1.70	-1.52	-1.60	-0.04	+0.55	-236.8
L 726	IV-19	250.436600	36.390942	13.68	11.104	2.36	4570	1.55	-1.54	1.55	-1.56	-1.52	+0.26	+0.16	-243.9
L 793	...	250.441763	36.451073	13.68	11.198	2.34	4660	1.65	-1.59	1.50	-1.53	-1.65	+0.54	-0.13	-248.5
K 699	X 24	250.657823	36.403545	13.75	11.249	2.32	4640	1.65	-1.60	1.75	-1.62	-1.57	+0.22	+0.40	-249.3
L 677	IV-4	250.431585	36.429428	13.75	11.358	2.30	4750	1.70	-1.59	1.80	-1.48	-1.70	-0.06	+0.71	-250.2
L 18	...	250.313409	36.490002	13.78	11.206	2.32	4570	1.60	-1.65	1.80	-1.64	-1.66	+0.10	+0.11	-249.5
L 800	IV-18	250.443097	36.386150	13.80	11.295	2.30	4635	1.65	-1.59	1.70	-1.74	-1.44	+0.29	+0.24	-246.3
L 1032	I-76	250.478956	36.461700	13.81	11.345	2.29	4600	1.60	-1.59	1.60	-1.69	-1.49	-0.19	-0.08	-246.0
L 871	I-19	250.449600	36.509624	13.89	11.396	2.26	4645	1.70	-1.62	1.70	-1.56	-1.67	-0.84	+0.63	-251.8
L 955	IV-22	250.459900	36.394932	13.92	11.382	2.26	4605	1.70	-1.54	1.55	-1.55	-1.52	+0.09	+0.29	-242.2
L 609	...	250.426025	36.439865	13.96	11.512	2.23	4690	1.75	-1.69	1.85	-1.67	-1.71	+0.39	+0.47	-251.2
L 81	II-23	250.353205	36.504230	13.97	11.474	2.23	4645	1.75	-1.60	1.60	-1.62	-1.57	+0.02	+0.56	-245.3
L 1001	I-49	250.468308	36.477646	13.99	11.606	2.21	4755	1.80	-1.54	1.80	-1.53	-1.54	+0.24	-0.06	-257.8
K 422	...	250.401823	36.285603	14.02	11.568	2.21	4690	1.75	-1.54	1.65	-1.55	-1.52	+0.44	+0.22	-244.0
L 1060	I-65	250.493449	36.475334	14.05	11.692	2.18	4785	1.85	-1.57	1.60	-1.56	-1.58	-0.08	+0.21	-236.5
L 162	III-43	250.378740	36.425434	14.09	11.603	2.18	4655	1.80	-1.48	1.40	-1.43	-1.52	-0.08	+0.08	-247.1
L 488	...	250.416136	36.488148	14.11	11.633	2.17	4665	1.80	-1.55	1.45	-1.63	-1.46	+0.20	+0.25	-243.0
L 1051	IV-78	250.488983	36.422718	14.12	11.653	2.17	4675	1.80	-1.57	1.65	-1.64	-1.49	-0.29	+0.37	-243.8
L 1114	...	250.541079	36.373940	14.12	11.905	2.13	4935	1.95	-1.65	1.65	-1.71	-1.59	+0.30	+0.01	-255.4
L 557	...	250.420067	36.569859	14.13	11.657	2.16	4670	1.80	-1.58	1.50	-1.61	-1.55	+0.45	-0.21	-247.9
L 79	...	250.352099	36.493851	14.18	11.809	2.13	4770	1.90	-1.55	1.40	-1.51	-1.59	+0.55	-0.26	-242.4
K 659	...	250.568872	36.416309	14.24	11.801	2.12	4700	1.85	-1.39	1.50	-1.47	-1.30	-0.01	+0.33	-240.9
L 140	III-25	250.375557	36.443192	14.24	12.242	2.05	5195	2.50	-1.61	1.50	-1.57	-1.64	+0.11	+0.61	-237.2
K 674	...	250.588623	36.564819	14.26	12.147	2.06	5055	2.05	-1.59	1.80	-1.61	-1.56	+0.69	+0.26	-249.0
L 787	I-2	250.440208	36.529823	14.26	11.903	2.09	4785	1.90	-1.58	1.65	-1.53	-1.63	+0.30	+0.47	-246.2
L 1050	...	250.489252	36.387623	14.29	11.893	2.09	4745	1.90	-1.47	1.70	-1.47	-1.46	+0.07	...	-245.7
L 1072	IV-80	250.501614	36.423615	14.31	11.973	2.07	4805	1.95	-1.55	1.70	-1.57	-1.52	+0.10	+0.64	-244.9
L 423	II-7	250.410956	36.510258	14.31	11.938	2.08	4770	1.95	-1.51	1.50	-1.48	-1.54	+0.51	-0.11	-237.1
L 824	I-39	250.444099	36.490067	14.34	12.094	2.05	4905	2.00	-1.56	1.70	-1.46	-1.65	+0.31	+0.37	-240.4
L 1096	I-67	250.513947	36.486725	14.40	12.048	2.04	4790	2.00	-1.58	1.40	-1.58	...	-0.07	+0.33	-250.9
L 1097	...	250.514202	36.505070	14.40	12.061	2.04	4805	2.00	-1.48	1.55	-1.50	-1.46	-0.32	+0.30	-256.2

Table 1—Continued

Star Name ^a	Alt. Name	RA J2000	DEC J2000	V	K _S	log(L/L _⊙)	T _{eff} (K)	log(g) (cgs)	[Fe/H] avg.	vt km s ⁻¹	[FeI/H]	[FeII/H]	[O/Fe]	[Na/Fe]	RV km s ⁻¹
L 29	II-63	250.323850	36.491638	14.51	12.186	1.99	4820	2.05	-1.59	1.80	-1.60	-1.58	...	+0.52	-237.9
K 224	J 37	250.275644	36.422974	14.52	12.225	1.98	4850	2.05	-1.53	1.55	-1.51	-1.54	+0.38	+0.50	-246.3
L 137	...	250.373757	36.537121	14.58	12.315	1.95	4880	2.10	-1.47	1.30	-1.42	-1.52	+0.22	+0.40	-245.1
L 16	J50	250.312979	36.398304	14.60	12.388	1.94	4940	2.15	-1.61	1.70	-1.53	-1.69	+0.44	-0.18	-245.3
K 647	...	250.546518	36.306267	14.71	12.488	1.89	4930	2.20	-1.58	1.70	-1.61	-1.55	-0.07	+0.07	-244.0
L 93	III-40	250.361839	36.424629	14.85	12.654	1.83	4960	2.25	-1.42	2.10	-1.35	-1.49	+0.42	+0.39	-245.8
L 1095	I-69	250.513806	36.465366	14.92	12.663	1.82	4400	1.30	-1.62	1.90	-1.62	-1.61	+0.32	-0.06	-242.0
L 6	J11	250.291419	36.502876	15.00	14.352	1.70	4450	1.30	-1.68	1.85	-1.74	-1.62	-0.02	+0.36	-251.3
L 101	II-60	250.363988	36.491802	15.09	13.027	1.72	4500	1.40	-1.68	1.80	-1.66	-1.69	+0.40	-0.32	-243.6
L 32	II-64	250.327637	36.478725	15.12	12.937	1.73	4850	2.10	-1.44	2.00	-1.34	-1.54	+0.01	+0.50	-242.3
CM 12	...	250.556994	36.554123	15.28	13.122	1.66	5000	2.45	-1.39	1.70	-1.28	-1.50	+0.74	-0.01	-235.5

^aDesignations from Ludendorf (1905) and Kadla (1966).